Cytoplasmic Microtubule Organizing Centers Regulate Meiotic Spindle Positioning in Mouse Oocyte

Running title: mcMTOCs regulate spindle positioning

DANIELA LONDONO VASQUEZ[1], KATHERINE RODRIGUEZ-LUKEY[1], SUSANTA K. BEHURA[1] & AHMED Z. BALBOULA[1,2]

1) Animal Sciences Research Center, University of Missouri, Columbia, MO 65211, USA

2) University of Cambridge, Department of Genetics, Downing Street, Cambridge, CB2 3EH, UK

Keywords: MTOC, Microtubule, Oocyte, Meiosis, Spindle positioning

ABSTRACT

During oocyte meiosis, migration of the spindle and its positioning must be tightly regulated to ensure elimination of the polar bodies and provide developmentally competent euploid eggs. Although the role of F-actin in regulating these critical processes has been studied extensively, little is known whether microtubules (MTs) participate in regulating these processes. Here, we characterize a pool of MTOCs in the oocyte that does not contribute to spindle assembly but instead remains free in the cytoplasm during metaphase I (metaphase cytoplasmic MTOCs; mcMTOCs). In contrast to spindle pole MTOCs, which primarily originate from the perinuclear region in prophase I, the mcMTOCs are found near the cortex of the oocyte. At nuclear envelope breakdown, they exhibit robust nucleation of MTs, which diminishes during polar body extrusion before returning robustly during metaphase II. The asymmetric positioning of the mcMTOCs provides the spindle with a MT-based anchor line to the cortex opposite the site of polar body extrusion. Depletion of mcMTOCs, by laser ablation, or manipulating their numbers, through inhibitors or inducers of autophagy, revealed that the mcMTOCs are required to regulate the timely migration and positioning of the spindle in meiosis. We discuss how forces exerted by F-actin in mediating movement of the spindle to the oocyte cortex are balanced by MT-mediated forces from the mcMTOCs to ensure spindle positioning.

INTRODUCTION

Mammalian oocytes enter meiosis during early fetal life. Soon after birth, meiotic oocytes undergo a lengthy arrest at the dictyate stage of the prophase I of the first meiotic division (MI) [1]. At the age of puberty, gonadotropin cues allow prophase I-arrested oocytes to resume MI evident by breakdown of the nuclear envelope (NEBD) and formation of a central bipolar spindle [2-4]. The central positioning of the spindle is required to establish proper kinetochore-MT attachments and to protect against aneuploidy. The position of the spindle dictates the plane of cell division [5] and therefore, in contrast to mitotic cells where a centrally positioned spindle allows symmetrical cell division, the meiotic spindle must migrate towards the cortex for the highly asymmetric meiotic divisions [5,6]. Such peripheral positioning of the spindle is critical to extrude the tiny polar body (PB) thereby retaining the great majority of the cytoplasm containing maternal RNAs and protein for the egg to support early embryonic development [7,8]. It is essential to understand the critical events of spindle positioning and migration, which are required for the fidelity of chromosome transmission to the next generation.

To date, F-actin and its regulatory molecules represent the only cytoskeletal components known to regulate spindle migration and positioning in the mammalian oocyte. It has been shown that perturbation of F-actin, but not of MTs, impairs spindle migration in oocytes and that the resulting increased symmetry of cell division results in infertility [6,9-11]. This contrasts with mitotically dividing somatic cells, where positioning of the spindle at the center of the cell is primarily regulated by the interaction of the astral MTs at its poles with the cell cortex [12]. Such astral MTs are nucleated by centrosomes, centriole pairs surrounded by peri-centriolar material (PCM). By contrast, mammalian oocytes lack classic centrosomes [13] because centrioles are lost

during early oogenesis through an unknown mechanism. The numerous acentriolar MT organizing centers of the oocyte (MTOCs) [13,14] are still able to nucleate astral-like MTs but these are short and unable to extend to the cortex when the spindle is centrally positioned [14-16]. These observations have enforced the notion that MTs have no role in regulating central spindle positioning and migration. It is therefore surprising that when mouse oocytes are treated with nocodazole, a MT depolymerizing agent, chromosomes migrate towards the cortex at a higher speed and at an earlier time than in control oocytes [11,17]. These unexplained observations suggest that MTs have, yet unknown, role(s) in regulating spindle migration and positioning in mammalian oocytes.

In prophase I-arrested oocytes, the MTOCs are initially found in the perinuclear region [13]. Then, before NEBD, these perinuclear MTOCs undergo distinct processes of decondensation, stretching and redistribution into a large number of smaller MTOCs [18,19]. The fragmented MTOCs are then clustered and sorted to form two poles necessary to assemble a bipolar spindle [14,20,21]. Another pool of MTOCs is also present in the cytoplasm during NEBD. Some of these cytoplasmic MTOCs migrate from the periphery to the center of the egg, where they participate in spindle formation [14,18]. Another subset of cytoplasmic MTOCs, hereafter referred to as metaphase cytoplasmic MTOCs (mcMTOCs) does not contribute to spindle formation and has yet unknown biological significance for oocyte meiosis.

Here, we show that the pMTOCs and the mcMTOCs of MI oocytes represent two different functional sets. We find by 3D time-lapse imaging that mcMTOCs localize asymmetrically opposite the site of F-actin enrichment where the polar body is extruded. Super-resolution

Stimulated Emission Depletion (STED) microscopy reveals that mcMTOCs are able to nucleate MTs that connect the spindle to the cortex. Importantly, we show that by increasing mcMTOC numbers following treatment with an inhibitor of autophagy or by depleting them by laser ablation, the meiotic spindle becomes abnormally positioned leading to aneuploidy. Our results suggest a model whereby the role of F-actin in mediating movement of the meiotic spindle to the cortex is balanced by forces exerted from mcMTOCs to ensure the timely migration and accurate positioning of the spindle in the oocyte.

RESULTS

MTOCs in the cytoplasm and at the spindle poles of meiotic oocytes

The multiple MTOCs of prophase I-arrested oocytes follow distinct patterns of behavior. Immediately before NEBD, perinuclear MTOCs become fragmented in three phases; decondensation, stretching and repositioning towards the spindle poles through the sequential actions of Polo-like kinase 1, BicD2-anchored dynein, and the KIF11 motor protein [18,19]. Soon after NEBD, a second group of cytoplasmic MTOCs migrates from the periphery to the center of the oocyte, where it participates with perinuclear MTOCs in spindle assembly [14,18]. Finally, a third population of MTOCs persists in the cytoplasm of MI oocytes at metaphase (here termed mcMTOCs) [16,22-25], whose role in meiosis is unknown. To follow the behavior of mcMTOCs during MI, we employed live imaging using 3D confocal microscopy to visualize prophase I-arrested oocytes (collected from CF-1 mice) expressing GFP-tagged Aurora A Kinase (AURKA-GFP, an integral component of MTOCs in mouse oocytes [26-28] and H2B-mCherry (H2B-mCh) to label MTOCs and DNA, respectively. As previously reported, perinuclear MTOCs became

fragmented into small multiple MTOCs at NEBD before they sorted and re-clustered at the two spindle poles as pMTOCs (Fig. 1A; Supplementary Movie 1). We also observed cytoplasmic MTOCs in the cytoplasm at NEBD, some of which migrated towards the oocyte center to contribute to spindle formation alongside pMTOCs whereas others, mcMTOCs remained free in the cytoplasm during prophase and metaphase I (Met I) after the bipolar spindle had formed (Fig. 1A; Supplementary Movie 1). We carried out 3D reconstruction of entire oocytes to examine the number (Fig. 1 B,C) and volume (Fig. D, E) of the mcMTOCs (Supplementary Movie 2). In contrast to pMTOCs which undergo a time-dependent decrease in number and increase in volume (due to MTOC clustering) as the oocyte proceeds to Met I, the mcMTOCs displayed the opposite pattern and showed a time-dependent increase in number and volume in prophase and Met I (Fig. 1A,B,D; Supplementary Movies 1 and 2). Each oocyte had a variable number of mcMTOCs (between 4 and 12) at Met I located on different focal planes (Supplementary Movie 3). The mcMTOCs became less distinct, appearing to be decreased in number and volume during anaphase I (Ana I) and telophase I (Telo I) before regaining their metaphase appearance as the oocytes arrested in Met II (Fig. 1A-E; Supplementary Movies 1 and 2). We confirmed that these AURKA-positive foci were indeed MTOCs by showing the colocalization of γ-tubulin, another integral component of PCM in meiotic oocytes [20] (Supplementary Fig. 1). To confirm our observations, we fixed CF-1 oocytes at different developmental stages (GV, Met I, Ana I/Telo I and Met II) and immunostained them to reveal the MTOC markers, γ-tubulin, pericentrin and Cep192 [18,29-31]. This also revealed pMTOCs and mcMTOCs at Met I (Fig. 1F, G) that were able to nucleate asters of MTs (α-tubulin staining, Fig. 1F). Similar findings were observed in Met I oocytes from C57BL/6 mice (Supplementary Fig. 2). Just as we observed in time-lapse imaging

of MTOCs in living oocytes, the mcMTOCs became less distinct in fixed preparations of oocytes in Ana I/Telo I of fixed MI oocytes.

mcMTOCs undergo three patterns of directional movement during MI

To dissect the directional motion and kinetics of the mcMTOCs, we tracked their movement in 3D reconstructions over time during pro-Met I. In contrast to pMTOCs which primarily originate from perinuclear MTOCs at NEBD, the mcMTOCs formed at the periphery of the oocyte (Fig. 2A; Supplementary Movie 4 and 5) and then appeared to undergo three phases of directional movement. In the first phase, from NEBD to early Met I, the peripheral mcMTOCs moved towards the oocyte's center with an average speed of 0.09 ± 0.007 μm min^{-1} and a maximum speed of 0.18 ± 0.005 μm min^{-1}. During this phase, the average volume of the mcMTOCs increased, in some cases due to mcMTOCs merging with each other (Fig. 2A; Supplementary Movie 4 and 5). The second was marked by the slowing of mcMTOC movement to an average speed of 0.06 ± 0.009 μm min^{-1} allowing them to remain in confined areas of the cytoplasm (Fig. 2B; Supplementary Movie 4). During this phase, the pMTOCs underwent active clustering whereas the mcMTOCs remained apart. The third phase occurred during Ana I and Telo I when the mcMTOCs showed a reversal of their behavior in phase I; they displayed a drastic reduction in volume and migrated towards the cortex with an average speed of 0.12 ± 0.01 μm min^{-1} and a maximum speed of 0.22 μm min^{-1} (Fig. 2C; Supplementary Movies 4 and 6). In as many as 50% of oocytes (14/28), we were not able to observe mcMTOCs during Ana I/Telo I but in all cases when they could be observed, the mcMTOCs migrated towards the region of cortex opposite direction the site of extrusion of the first PB. The mcMTOCs showed independent directional movement to cytoplasmic droplets and so do not reflect overall

cytoplasmic movements (Supplementary Fig. 3). Taken together, our observations confirm that meiotic oocytes have two different pools of MTOCs and suggest that mcMTOCs differ from pMTOCs in their function.

mcMTOCs localize asymmetrically to anchor the spindle to the cortex

To determine whether the mcMTOCs were physically connected to pMTOCs, we employed immunocytochemistry and STED super-resolution microscopy to visualize the MTOCs in relation to MTs and F-actin. We confirmed that F-actin formed a cage around the spindle as previously reported [10,32] but could not detect any direct connection of F-actin between the pMTOCs and mcMTOCs (Supplementary Fig. 4). In contrast, we detected MTs originating from the mcMTOCs and linking them to both the oocyte cortex and the pMTOCs and spindle (Fig. 3A,B). In addition, we also observed MTs connecting mcMTOCs with each other. Relatively short astral-like MTs could not reach the oocyte cortex unless they bind mcyMTOCs (Fig. 3A,B). Thus, mcMTOCs enable MTs to bridge the gap between the spindle and the cortex. It was also evident from our observations that the mcMTOCs were asymmetrically distributed in the oocyte cytoplasm leading us to consider their relationship in time and space to the positioning of the spindle itself. In prophase arrest oocytes, the GV is usually found in a centralized location [33-36]. Consequently, the spindle also forms around the chromatin at or near the center of the oocyte before it migrates towards the cortex in late pro-Met to allow asymmetrical cell division. In all the oocytes examined, we found that the mcMTOCs were all asymmetrically positioned from the GV stage and throughout NEBD and early pro-Met I when the spindle is still localized centrally (Fig. 3C; Supplementary Movie 7). Strikingly, when the spindle began its actin-mediated migration, this took place towards the opposite side of the

oocyte to that occupied by mcMTOCs in the majority of the oocytes (38 out of 40 examined, Fig. 3 C-E). These findings suggest a model whereby mcMTOCs localize asymmetrically to anchor the spindle to the cortex in such a way as to oppose the F-actin mediated force that builds to direct the spindle to the cortex on the opposite face of the oocyte for polar body extrusion. This would account for the unexplained finding that nocodazole-induced MT depolymerization during Met I results in the earlier migration of chromosomes towards the cortex at a relatively higher speed than in control oocytes (Supplementary Fig. 5) and others [11]. Thus, the mcMTOCs appear to enable opposing MT forces that counter spindle/chromosome migration that are necessary to regulate its timing and the final position of the spindle.

mcMTOCs regulate spindle positioning in acentriolar oocytes

To determine the function(s) of mcMTOCs during MI and to test the above hypothesis, we selectively depleted mcMTOCs by two-photon laser ablation (Fig. 4A). The two-photon laser microscope has the advantage of offering deeper tissue penetration enabling efficient ablation and minimizing off-target effects [37]. We first microinjected prophase I-arrested oocytes with cRNAs encoding *Aurora A-GFP* and *eGFP-EB3* to label MTOCs and MTs, respectively. We then marked small cuboidal regions surrounding each mcMTOC, which we then exposed to a 927 nm wavelength laser to ablate the mcMTOCs, (Fig. 4B; Supplementary Movie 8). We ensure reduction of fluorescence of each mcMTOC to background levels (compare images before ablation, Fig. 4B, upper panels, to after ablation, Fig. 4B, lower panels) before ablating the next. Importantly, laser ablation not only depleted the mcMTOCs but also disrupted their associated nucleation of MTs (Fig. 4C). We also exposed control oocytes to the same protocol by ablating random areas of the cytoplasm adjacent to but not overlapping with the mcMTOCs.

We confirmed the efficiency of mcMTOC depletion by immunostaining a subset of oocytes to reveal γ-tubulin and were only able to detect γ-tubulin foci in the cytoplasm but not at spindle poles (Supplementary Fig. 6). Control and mcMTOC-depleted oocytes were *in vitro* matured for 16 h allowing us to assess the proportion of Met II eggs and determine their karyotype using an *in situ* chromosome counting technique [38,39]. We first noted that the depletion of mcMTOCs resulted in a significant increase in oocytes arrested at Met I compared to control oocytes (Fig. 4D). Importantly, a relatively higher proportion of mcMTOC-depleted eggs were aneuploid (7 out of 13 examined eggs) compared to controls (6 out of 24 examined eggs). Because depletion of mcMTOCs increased the percentage of oocytes arrested at Met I stage (Fig. 4D), we were not able to assess spindle positioning due to the high variability related to the meiotic stage and so we chose to arrest meiotic progression in Met I by incubating oocytes in meiotic maturation medium containing a proteasome inhibitor (MG-132). In this way, we could compare spindle positioning in such arrested oocytes (Fig. 4A). This revealed that whereas in control MI arrested oocytes, the spindle maintained its position over a period of 8h, the position of the spindle in mcMTOC-depleted oocytes was not stable (Fig. 4e; Supplementary Movie 9 and 10) and displayed considerable movement (Fig. 4F,G). Following the onset of spindle movement in mcMTOC-depleted oocytes, the spindle poles lost their integrity in contrast to control oocytes, likely due to the imbalance of forces on spindle poles (Supplementary Movie 9 and 10). Together this suggests that the mcMTOCs are required to position the MI spindle and maintain the integrity of the spindle poles.

Autophagy regulates mcMTOC numbers and spindle positioning in meiotic oocytes

In mitotic cells, autophagy plays an important role in regulating and maintaining the proper number of centrosomes where autophagy-deficient cells contained multiple centrosomes [40,41]. This led us to investigate the effects of inhibiting or inducing autophagy upon mcMTOC numbers and the consequences for meiosis. To this end, we chose to treat oocytes with 3-Methyladenine (3-MA), which inhibits autophagy by blocking autophagosome formation via the inhibition of type III Phosphatidylinositol 3-kinases (PI-3K). However, because 3-MA (autophagy inhibitor) blocks NEBD (data not shown), we treated oocytes with 3-MA immediately after NEBD. We also treated oocytes with rapamycin as an inducer of autophagy by adding the compound to the *in vitro* maturation medium during prophase I. In both cases, we allowed the treated oocytes (3-MA or rapamycin) together with controls to mature for 5 h post-NEBD prior to fixation and immunostaining using anti-Cep192 and anti-α-tubulin antibodies to label MTOCs and the spindle, respectively. We found that treatment with rapamycin resulted in a decrease in the number of mcMTOCs, compared to control oocytes (Fig. 5A-C). In contrast, treatment with 3-MA significantly increased the number of mcMTOCs, but not pMTOCs, compared to control oocytes (Fig. 5d-f). To determine the effect of such drug treatments upon spindle positioning, we used DIC imaging to track the position of chromosomes over time. Rapamycin-treated oocytes behaved in a similar way to controls; we could see no significant differences in the proportion of oocytes completing MI and extruding a polar body (Fig. 6A,B). Moreover, rapamycin-treated oocytes showed no differences to controls in chromosome positioning (Fig. 6A,F; Supplementary Movie 11 and 12**)**, in the average time spent by chromosomes during migration to reach the cortex (Fig. 6C), in the total distance traveled by chromosomes until reaching the cortex; Fig. 6D), or in the average speed of migrating

chromosomes (Fig, 6E). By contrast, the increase in MTOC numbers following 3-MA treatment was associated with abnormal chromosome (spindle) positioning and orientation (Fig. 6A,F; Supplementary Movie 13 and14) with chromosomes moving in circles in around 40% of oocytes treated with 3-MA. Accordingly, we found a significant increase in the distance traveled by chromosomes during migration until reaching the oocyte cortex (Fig. 6D). In line with our model that mcMTOC-mediated MTs anchor the spindle to the cortex opposite the PBE side to position the spindle centrally, we found that increasing mcMTOC numbers by 3-MA treatment resulted in a significant delay in chromosome migration towards the cortex (Fig. 6C), resulting from their significantly ($p < 0.001$) reduced speed (Fig. 6E) in comparison to control oocytes. Indeed, we observed cases in which the chromosomes underwent segregation before the spindle had reached the cortex, resulting in enlarge polar bodies in around 21.05% of oocytes (Supplementary Movie 14). The relatively weaker effect of rapamycin than 3-MA on spindle positioning could be attributed to our observation that average mcMTOC number in rapamycin-treated oocytes (~ 4) remained within the range of mcMTOC numbers in control oocytes (between 4 and 12). Together, these data show that mcMTOC numbers must be regulated tightly, and provide further evidence that mcMTOCs play an important role in regulating the spindle position and timing of its migration in mouse oocytes.

DISCUSSION

To date, the only known function of acentriolar MTOCs in mouse oocytes is to assemble the spindle. Using 3D time-lapse confocal microscopy, we identify a subset of MTOCs that remain free in the cytoplasm during Met I of meiosis and which do not contribute to bipolar spindle assembly *per se*. In contrast to polar pMTOCs, which originate mainly from the perinuclear

MTOCs in prophase I, the mcMTOCs originate exclusively from MTOCs present in the cytoplasm in prophase I. The mcMTOCs are first observed near the oocyte cortex at NEBD; they increase in number and size while moving to a central position during Met I. STED super-resolution microscopy revealed that microtubules nucleated by the mcMTOCs connect one side of the spindle to the cortex during Met I. In Ana I/Telo I of MI, the mcMTOCs undergo a decrease in both number and size while migrating towards the cortex. When mcMTOCs functions were perturbed, either by laser ablation or treatment with 3-Methyladenine (3-MA) to inhibit type III Phosphatidylinositol 3-kinases and increase MTOC numbers, we have shown that the mcMTOCs play a role in regulating spindle positioning and the timing of its migration to the cortex.

To our knowledge, this is the first study of the function of mcMTOCs in living mammalian oocytes, which differ in several ways from the pMTOCs. The majority of pMTOCs, for example, originate from the perinuclear MTOCs, which never contribute to the mcMTOCs. Whereas the pMTOCs undergo a clustering-associated decrease in number and increase volume During pro-Met I/Met I, the mcMTOCs undergo a steady increase in both number and volume and rarely self-aggregate (~1.5% of all examined mcMTOCs). Interestingly, inhibition of autophagy with 3-MA increased the number of mcMTOCs, but not pMTOCs. Finally, in contrast to pMTOCs, mcMTOCs participated in spindle positioning but never contributed to bipolar spindle assembly. Together, these observations suggest that mammalian oocytes have two different functional sets of MTOCs and raise the future important challenge to determine whether differences in their biochemical compositions underlie their differences in function.

The primary function of the spindle is to provide the machinery for faithful chromosome segregation. This is achieved in a series of critical, non-overlapping steps. First, during pro-Met I and early Met I, the spindle is assembled and positioned at or near the oocyte's center. Second, during the late Met I, the spindle migrates towards a sub-cortical location to allow asymmetrical cell division. Third, the spindle rotates from a parallel to a perpendicular position in relation to the cortex to allow PB extrusion. Many studies have emphasized the roles of F-actin and its motor proteins in regulating spindle positioning and migration [9-11] and two models have been proposed to explain how F-actin regulates spindle positioning and migration. In the first, F-actin enrichment at the cortex provides a spindle pulling force [9]. In the second, a spindle pushing force is mediated by the cytoplasmic F-actin meshwork [11]. Both models enforce the notion that an F-actin-mediated force on the spindle, whether pushing or bulling, acts towards the nearest cortical side through which the PB is extruded. On the other hand, spindle orientation seems to be dependent on both F-actin and MTs [15]. Astral-like MTs are only able to reach the cortex only when it is very close to the spindle poles [15]. Because astral-like MTs are relatively short and cannot easily reach the cortex, they can only establish contacts with MTs nucleated by mcMTOCs which, in turn, could act as amplifying sites that anchor the spindle to the cortex. This model, which we here propose, thus depends on the presence of two opposing forces: cyMTOC-mediated MTs at one side and F-actin at the other side of the spindle (Fig. 6). These opposing forces would be essential to position the spindle centrally during early Met I and to prevent premature spindle migration. Our model is consistent with three sets of observations: 1) mcMTOCs are exclusively localized asymmetrically, opposite the site of PB extrusion (the side of F-actin enrichment); 2) mcMTOCs undergo a significant decrease in number and volume during late Met I and Ana I/Telo I, allowing the F-actin mediated force to extrude the PB; and 3)

313 nocodazole-mediated MT depolymerization advances the timing of chromosome migration to the
314 cortex, which takes place at a relatively higher speed [11,17] whereas increasing mcMTOC numbers
315 delays chromosome migration to the cortex, which occurs at a relatively reduced speed compared
316 to controls.
317
318 Depletion of mcMTOCs, disruption of mcMTOC numbers and MT depolymerization were each
319 associated with abnormal spindle positioning and/or perturbed chromosome/spindle migration.
320 For example, increasing mcMTOC numbers by 3-MA treatment significantly decreased
321 chromosome speed and delayed chromosome migration towards the cortex. This phenotype
322 accords with increased mcMTOC-mediated MT forces that oppose F-actin; thereby preventing
323 proper spindle migration. Conversely, depleting mcMTOCs using laser ablation or MT
324 depolymerization has the reciprocal effect [11,17]. These findings indicate that the numbers of
325 mcMTOCs must be regulated tightly to regulate spindle positioning and timely spindle
326 migration.
327
328 In almost all mammals, including humans [42,43], meiotic oocytes contain numerous acentriolar
329 MTOCs. This is in contrast to somatic mitotic cells, which contain only a pair of centrosomes
330 that are sufficient to assemble and position the spindle centrally. Positioning the spindle at the
331 center of mitotic cells depends on nucleating symmetrical astral MTs that anchor the spindle to
332 the cell cortex. However, the mechanism appears different during MI. Mammalian eggs are large
333 and the astral MTs from acentriolar MTOCs are relatively short. Yet, the cell must divide
334 asymmetrically, something that would likely be difficult for a pair of symmetrical centrosomes to

335 achieve. Our proposed model may, therefore, account for why meiotic oocytes rely upon two
336 different functional sets of numerous MTOCs rather than a pair of typical centrosomes.
337
338 **MATERIAL AND METHODS**
339 **Ethics**
340 All animals were kept and experiments were conducted in accordance with UK Home Office
341 regulations and the University of Missouri (Animal Care Quality Assurance Ref. Number, 9695).
342
343 **Oocyte collection, microinjection and culture**
344 Full-grown GV-arrested oocytes were isolated from CF-1 or C57BL/6 female mice (6-8-week-
345 old) previously primed (~44 h before collection), with pregnant mare serum gonadotropin (Lee
346 BioSolutions #493-10-10) according to [44,45]. Unless otherwise specified, CF-1 mice were used to
347 conduct the experiments. Cumulus oocyte complexes (COCs) were collected and denuded using
348 mechanical pipetting in bicarbonate-free minimal essential medium (MEM) containing 3 mg/ml
349 polyvinylpyrolidone (PVP) and 25 mM Hepes (pH 7.3) supplemented with 2.5 μM milrinone
350 (MilliporeSigma, St. Louis, MO, USA # M4659), a phospho diesterase inhibitor to arrest the
351 oocytes at prophase I [46]. Prophase I-arrested oocytes were microinjected with 10-15 pl of cRNAs
352 encoding fluorescently labeled proteins while cultured in milrinone-containing MEM medium.
353 Microinjected oocytes were then cultured in Chatot, Ziomek, and Bavister (CZB) medium [47]
354 supplemented with milrinone in a humidified incubator with 5% CO_2 in air at 37°C for ~3 h to
355 allow protein expression before releasing into milrinone-free CZB medium and initiating *in vitro*
356 maturation. Met I, Ana I/Telo I or Met II oocytes were collected at 4, 7 or 14 h after NEBD.

Nocodazole (MilliporeSigma #M1404), MG-132 (MilliporeSigma #474790), Rapamycin (Enzo Life Sciences, Farmingdale, NY, USA #BML-A275), 3-Methyladenine (3-MA, Cayman Chemical, Ann Arbor, MI, USA #13242) were dissolved in dimethyl sulfoxide (DMSO) and used at a final concentration of 7.5 µM, 20 µM and 10 mM, respectively. *In vitro* maturation was carried out in organ culture dishes under humidified conditions (Becton Dickinson #353037).

Cloning and *in vitro* cRNA synthesis

Generation of *Aurka-Gfp*, *H2b-mCherry* and *eGfp-Eb3* were described previously [28,48]. DNA linearization of *Aurka-Gfp* and *H2b-mCherry* constructs was carried out using Nde I (New England BioLabs), whereas DNA linearization of *eGfp-Eb3* construct was carried out using SfiI (New England BioLabs). Purification of linearized DNA was carried out according to the manufacturer's protocol (Qiagen, QIAquick PCR Purification). Purified DNA was *in vitro* transcribed using an mMessage mMachine T7 kit (Ambion) to generate *Aurka-Gfp* and *H2b-mCherry* cRNAs or mMessage mMachine T3 kit (Ambion) to generate eGfp-Eb3 cRNA according to the manufacturer's instructions. cRNA purification was performed using an RNAEasy kit (Qiagen) and stored at −80°C.

Immunocytochemistry and fluorescence microscopy

Meiotic oocytes were fixed for 20 min at room temperature in freshly prepared 2 % paraformaldehyde solution (MilliporeSigma #P6148) dissolved in phosphate buffer saline (PBS). Fixed oocytes were permeabilized in 0.1% Triton X-100 in PBS for 20 min prior to incubation for an additional 20 min in PBS containing 0.3% BSA and 0.01% Tween-20 (blocking solution). Primary antibody incubation was performed at room temperature for 1 h. Oocytes were then

washed three times (8-9 min each) prior to incubation with secondary antibodies for 1 h. Oocytes were washed again three times in blocking solutions for 8-9 min. To detect F-actin, phalloidin (Texas Red X Phalloidin, ThermoFisher Scientific #T7471; 1:50) was added to secondary antibody solutions. Oocytes were mounted on slides using Vectashieled with 4',6-Diamidino-2-Phenylindole, Dihydrochloride (DAPI; Vector Laboratories, Burlingame, CA, USA) to stain DNA. To label DNA for STED super-resolution imaging, 5 mg/m Hoechst 33342 was used (Molecular Probes H3570). The following primary antibodies were used in immunofluorescence: α-tubulin-Alexa Fluor 488 conjugate (Life Technologies #322 588; 1:100), Cep192 (Young In Frontier #AR07-PA0001; 1:100), γ-tubulin (Millipore-Sigma #T6557; 1:75), Pericentrin (BD Biosciences #611814; 1:100), CREST autoimmune serum (Antibodies Incorporated #15-234; 1:25). Omitting the primary antibody served as a negative control. Fluorescence signals were detected under a 63X objective using Leica TCS SP8 confocal microscope equipped with 3-color, 3-D STED super-resolution 3X system. Images were captured to span the entire oocyte at 3 µm Z-intervals (confocal microscopy) or 0.5 µm Z-intervals (STED super-resolution microscopy). All images were acquired using the same laser power when the intensity of fluorescence is quantified.

Time-lapse confocal microscopy

Oocytes expressing fluorescently labeled proteins were transferred to milrinone-free CZB medium and imaged over time under a 63X objective using Leica TCS SP8 confocal microscope equipped with microenvironmental chamber to maintain the oocytes at controlled CO_2 (5%) and temperature (37 °C) in a humidified air. DIC, GFP and mCherry image acquisitions were started at prophase I stage and images were captured every certain time according to each experimental

design (as indicated in corresponding figure legends). Images were captured to span the entire region including all MTOCs at 3 μm Z-intervals.

Depletion of mcMTOCs using laser ablation

Depletion of mcMTOCs was carried out using two-photon laser ablation which has the advantage of offering deeper tissue penetration, efficient ablation and minimizing off-target effects [37]. Two different microscopes were used. Oocytes expressing fluorescently labeled proteins were transferred to milrinone-free MEM medium and mcMTOCs were ablated using upright LaVision BioTec TriM Scope II (with controlled temperature at 37 °C) or to milrinone-free CZB medium if Leica TCP SP8 two-photon inverted microscope (equipped with microenvironmantal chamber to control CO_2 and temperature) was used. In both cases, a small square area(s) surrounding mcMTOCs were marked and then exposed to a laser with 927 nm wavelength. We compared the first image (before ablation) and the second image (after ablation) in the time series cycle to ensure that after ablation, the fluorescence in the targeted mcMTOCs decreased to that observed at the background levels. Next, we moved the focal plane and ablated the remaining mcMTOCs. McMTOC-depleted oocytes underwent live imaging using the same parameters. Control oocytes were exposed to the same protocol except ablating random areas of the cytoplasm, just adjacent and equal to the same size and number of mcMTOCs.

Image processing and analysis

Images acquired using 3-D STED super-resolution microscopy were deconvolved using Huygens Professional software before image analysis. NIH image J software (National Institute of Health, Bethesda, MD, USA) was used to process and analyze the images of fixed oocytes. The speed

and average distance of chromosome/spindle/MTOCs at their final position over time were analyzed using the manual tracking function of NIH image J software. The point of intersection between the line connecting the two dominant spindle poles and spindle midzone was used to determine the position of the spindle. The point of intersection between the two lines representing the minor axis length and the major axis length of chromosomes was used to determine the position of all chromosomes [49]. The speed and distance for each MTOC were analyzed separately before calculating the average for all MTOCs within each oocyte. 3D reconstruction of MTOCs, MTOC number and volume were processed and analyzed using isosurface spot analysis feature of Imaris software (Bitplane, Zürich, Switzerland) according to [18]. Briefly, based on MTOC signal to noise, the threshold value was adjusted on an oocyte-to-oocyte basis followed by MTOC surface segmentation. MTOC number was calculated using the spot analysis feature, whereas MTOC volume was analyzed using surface analysis feature. mcMTOCs were quantified after excluding the pMTOCs manually, and *vice versa*. Same processing parameters were applied for each experimental analysis

In situ chromosome counting

Oocytes at Met II stage (12 h post-NEBD) were treated with 100 μM monastrol (MilliporeSigma #M8515), an Eg5-kinesin inhibitor to induce monopolar spindle formation with subsequent chromosome dispersion [38,39]. Oocytes were fixed and immunostained by Cep192, pericentrin, as previously mentioned with CREST autoimmune serum to detect kinetochores. Oocytes were then mounted onto a glass slide using Vectashield with DAPI (Vector Laboratories) to label DNA. Confocal microscopy was used to image the entire region of the chromosomes at 0.7-μm Z-

intervals to capture all kinetochores. Serial confocal sections were analyzed and the total number of kinetochores were counted using NIH image J software.

Statistical analysis

One-way ANOVA, Student t-test and chi-square contingency test were used to evaluate the differences between groups using GraphPad Prism. ANOVA test was followed by the Tukey post hoc test to allow the comparison among groups. The differences of $P < 0.05$ were considered significant. The data were expressed as means ± SEM.

FUNDING

This study was supported by Marie Sklodowska-Curie Fellowship 706170, Horizon 2020, European Commission and laboratory start-up funding from the University of Missouri to AZB.

ACKNOWLEDGMENTS

The authors would like to thank Dr. David Glover, California Institute of Technology, USA for critical reading and editing the manuscript, and for providing resources. The authors would like to thank all members of the Glover lab and the Balboula lab for valuable help and discussions.

DECLARATION OF INTEREST

The authors declare that there is no conflict of interest that could be perceived as prejudicing the impartiality of the research reported.

FIGURE LEGENDS

Figure 1: Two different sets of MTOCs are present in acentriolar oocytes. (A) Time-lapse confocal microscopy of MTOCs in live oocytes. Full-grown prophase-I oocytes were injected with cRNAs encoding *H2b-mCherry* (red) and *Aurka-Gfp* (pseudo white), incubated in milrinone-containing CZB medium for 3 h, followed by *in vitro* maturation. Shown are representative images (Z-projection of 16 sections every 3 μm) from a time course (see Supplemental Movie 1). Lower panels represent a 3D reconstruction of MTOCs from oocyte shown in upper panels (see Supplemental Movie 2). Fluorescence images were captured every 20 min (time, h:min). The scale bar represents 10 μm. The white arrow represents cytoplasmic MTOC that participate in spindle pole formation as a pMTOC. White arrowhead represents cytoplasmic MTOC that remains in the cytoplasm during Met I (mcMTOC). (B,D) Quantification of average MTOC number and MTOC volume over time during meiosis I, respectively. Error bars show S.D. Dashed blue lines represent the time of Ana I onset. (C,E). Quantification of average MTOC number and MTOC volume, respectively, during metaphase I (Met I) and anaphase I/telophase I (Ana I/Telo I) stages. The data are expressed as mean ± SEM. Student t-test was used to analyze the data. Values with asterisks vary significantly, ****P < 0.0001. The total number of analyzed oocytes (from three independent replicates) is specified above each graph. (F) Fully grown prophase-I-arrested oocytes were *in vitro* matured for 0 (Pro I, prophase I), 8 h (Met I), 9 h (Ana I/Telo I) or 16 h (Met II) prior to fixation and immunocytochemistry using γ-tubulin and α-tubulin antibodies to label MTOCs (red) and microtubules (grey). DAPI was used to detect DNA (blue). (G) Fully grown prophase-I-arrested oocytes were *in vitro* matured for 8 h (Met I) followed by fixation and immunostaining using Cep192 (red) and pericentrin (grey) antibodies to label MTOCs. DAPI was used to detect DNA

(blue). Shown are representative confocal z-projections. Arrowheads represent mcMTOCs. A total of 184 oocytes were examined. Scale bars represent 10 μm.

Figure 2: mcMTOCs exhibit three different directional behaviors during meiosis I. Tracking of 3D reconstructed mcMTOCs from time-lapse confocal microscopy in live oocytes during three different phases: (A) nuclear envelope breakdown (NEBD)- early metaphase I (Met I, see Supplemental Movie 4 and 5), (B) Met I (see Supplemental Movie 4) and (C) late Met I-telophase I (Telo I), see Supplemental Movie 5 and 6. Full-grown prophase-I oocytes were injected with cRNAs encoding *H2b-mCherry* (red) and *Aurka-Gfp* (pseudo white), incubated in milrinone-containing CZB medium for 3 h prior to *in vitro* maturation. Shown are representative images of 3D reconstructed Z-projection of 16 sections every 3 μm from a time course. Fluorescence images were captured every 15 min (time, h:min). The scale bar represents 20 μm. Right panels show a zoomed area of mcMTOC tracking over time. White arrows represent the overall direction of displacement calculated automatically by Bitplane Imaris software. Arrowheads represent mcMTOCs. The total number of analyzed oocytes is 34.

Figure 3: mcMTOCs anchor the spindle to the cortex. (A) Fully grown prophase-I-arrested oocytes were *in vitro* matured for 6 h (metaphase I) prior to fixation and immunocytochemistry using γ-tubulin and α-tubulin antibodies to label MTOCs (red) and microtubules (grey). Hoechst was used to detect DNA (blue). Fluorescence signals were detected under a 63X objective using STED super-resolution system. Shown is a representative image (Z-projection of 65 sections every 0.5 μm). (B) Example of fluorescence intensity of microtubules in "B", connecting pMTOCs, mcMTOCs and the cortex, using the 'plot profiles' function in

ImageJ. The scale bar represents 10 µm. (C) Representative images (Z-projection of 16 sections every 3 µm) of time-lapse confocal microscopy of a live oocyte expressing AURKA-GFP (MTOCs) and H2B-mCherry (chromosomes) from a time course (see Supplemental Movie 7). Fluorescence and bright-field images (lower panels) were captured every 20 min (time, h:min). Arrowheads represent mcMTOCs. Scale bars represent 10 µm. (D) Schematic diagram shows how the proportion of polar body extrusion side in relation to mcMTOC position was assessed. (E) Quantification of the proportion of polar body extrusion side from "C" according to "D". The data are expressed as mean ± SEM. Student t-test was used to analyze the data. Values with asterisks vary significantly, ****P < 0.0001. The total number of analyzed oocytes (from three independent replicates) is specified above the graph.

Figure 4: mcMTOCs are required to regulate spindle positioning in meiotic oocytes. (A) Schematic diagram shows the experimental design following mcMTOC depletion. (B-G) Oocytes expressing AURKA-GFP and eGFP-EB3 were *in vitro* maturated for 6 h (metaphase I, Met I), transferred to CZB medium with or without MG-132, followed by mcMTOC depletion using two-photon laser ablation. Small square area(s) surrounding mcMTOCs were marked and then exposed to a laser with 927 nm wavelength. Control oocytes were exposed to the same parameters except ablating random areas of the cytoplasm, just adjacent and equal to the same size and number of mcMTOCs. (B**)** Z-sections of 3D time-lapse imaging of a live oocyte during mcMTOC ablation (see Supplemental Movie 8). Black arrowheads represent mcMTOCs before ablation (upper panels). White arrowheads represent laser beam targets (middle panels). (C) Z-sections of 3D time-lapse imaging of live oocyte to track microtubules (eGFP-EB3) following mcMTOC ablation. Black arrow represents mcMTOC

before ablation (-3 S). Black arrowheads track microtubules over time. The scale bar represents 20 μm. (D) control and mcMTOC-depleted oocytes were *in vitro* matured in MG-132-free medium until Met II (16 h) and assessed for extrusion of the first polar body (PBE). The data are expressed as mean ± SEM. chi-square contingency test was used to analyze the data. Values with asterisks vary significantly, **P < 0.01. The total number of analyzed oocytes in each group (from two independent replicates) is specified above each condition within each graph. (E) Z-projection (16 sections every 3 μm) of 3D time-lapse microscopy of control (see Supplemental Movie 9) and mcMTOC-depleted (see Supplemental Movie 10) Met I oocytes while cultured in MG-132-containing medium for additional 9 h to track the spindle. Fluorescence images were captured every 3 min (time, h:min). White arrowheads represent the tracking path of all time periods. The scale bar represents 10 μm. (F) Quantification of total distance traveled by the spindle. (G) Quantification of average spindle speed. The data are expressed as mean ± SEM. Student t-test was used to analyze the data. Values with asterisks vary significantly, ****P < 0.0001. The total number of analyzed oocytes (from two independent replicates) is specified above each graph.

Figure 5: Autophagy regulates mcMTOC numbers in meiotic oocytes. (A) Full-grown prophase-I oocytes were divided into two groups and treated with DMSO or Rapamycin (added at 0 h after collection) followed by *in vitro* maturation until metaphase I (Met I, 7h). Met I oocytes were fixed and immunostained using Cep192 and α-tubulin antibodies to label MTOCs (red) and microtubules (grey). DAPI was used to detect DNA (blue). (B) Quantification of average mcMTOC number in "A". (C) Quantification of average pMTOC number in "A". (D) Full-grown prophase-I oocytes were divided into two groups and treated with DMSO or 3-MA

(added at NEBD) followed by *in vitro* maturation until metaphase I (Met I, 7h). Met I oocytes were fixed and immunostained using Cep192 and α-tubulin antibodies to label MTOCs (red) and microtubules (grey). DAPI was used to detect DNA (blue). (E) Quantification of average mcMTOC number in "D". (F) Quantification of average pMTOC number in "D". Arrowheads represent mcMTOCs. The data are expressed as mean ± SEM. Student t-test was used to analyze the data. Values with asterisks vary significantly, *P < 0.05, ****P < 0.0001. The total number of analyzed oocytes (from two independent replicates) is specified above each graph.

Figure 6: Autophagy regulates spindle positioning in meiotic oocytes.

(A) Z-projection (16 sections every 3 µm) of time-lapse imaging of DMSO, Rapamycin (Rap) and 3-MA-treated oocytes (see Supplemental Movie 11, 12, 13 and 14, respectively). Images were captured every 30 min. White arrows represent the direction of chromosome displacement. Scale bars represent 10 µm. Lower panels of each group show the tracking path (blue) over time. (B) Quantification of the percentage of first polar body extrusion (PBE). (C) Quantification of the average time spent by chromosomes from the start of migration till reaching the cortex. (D) Quantification of the total distance traveled by chromosomes from the start of migration until reaching the cortex. (E) Quantification of average chromosome speed during migration. (F) Quantification of the percentage of oocytes exhibiting abnormal spindle positioning and orientation prior to reaching the oocyte cortex. Arrows represent the direction of chromosome displacement. The data are expressed as mean ± SEM. One-way ANOVA was used to analyze the data. Values with asterisks vary significantly, *P < 0.05, ***P < 0.001, ****P < 0.0001. The total number of analyzed oocytes (from three independent replicates) is specified above each graph.

Figure 7: Schematic model for spindle positioning in the meiotic oocyte.

Supplementary Figure 1: AURKA-GFP foci colocalize with pericentriolar material protein (γ-tubulin) at mcMTOCs. Full-grown prophase-I oocytes were injected with *Aurka-Gfp* (green), incubated in milrinone-containing CZB medium for 3 h, followed by *in vitro* maturation. Metaphase I oocytes were fixed and immunostained using γ-tubulin antibody to label MTOCs (red). DAPI was used to detect DNA (blue). Shown are representative Z-projection of confocal images. The scale bar represents 10 μm.

Supplementary Figure 2: MTOCs in the cytoplasm and at the spindle poles of meiotic oocytes collected from C57BL/6 mice. Full-grown prophase-I oocytes collected from C57BL/6 mice were *in vitro* matured for 7 h. Metaphase I oocytes were fixed and immunostained using γ-tubulin and α-tubulin antibodies to label MTOCs (red) and microtubules (grey). DAPI was used to detect DNA (blue). Arrowheads represent mcMTOCs. Shown are representative Z-projection of confocal images. The scale bar represents 10 μm.

Supplementary Figure 3: mcMTOC movement does not follow the movement of the cytoplasm. Representative images (Z-projection of 16 sections every 3 μm) of time-lapse confocal microscopy of live oocytes expressing AURKA-GFP (MTOCs) and H2B-mCherry (chromosomes) from a time course. Fluorescence and bright-field images (lower panels) were captured every 15 min (time, h:min). The white arrow represents cytoplasmic droplet. Lower panels show the tracking of both cytoplasmic droplet (green) and mcMTOC (blue). The scale bar represents 10 μm.

610 **Supplementary Figure 4: F-actin localization in mouse oocytes.** Full-grown prophase-I
611 oocytes collected from C57BL/6 mice were *in vitro* matured for 7 h. Metaphase I oocytes were
612 fixed and immunostained using γ-tubulin to label MTOCs (red). Hoechst stain was used to detect
613 DNA (blue) and phalloidin stain was used to detect F-actin (pseudo green). Shown are
614 representative Z-projection. The scale bar represents 10 μm.
615
616 **Supplementary Figure 5: Inhibition of MTs accelerates chromosome migration towards the**
617 **cortex in meiotic oocytes.** Full-grown prophase-I oocytes were divided into two groups and
618 treated with DMSO or nocodazole (added at 0 h after collection) followed by *in vitro* maturation
619 and time-lapse imaging. Images were captured every 15 min. (A) Quantification of the average
620 time spent by chromosomes until reaching the cortex. (B) Quantification of average chromosome
621 speed during migration. The data are expressed as mean ± SEM. Student-t test was used to
622 analyze the data. Values with asterisks vary significantly, ***$P < 0.001$, ****$P < 0.0001$. The
623 total number of analyzed oocytes (from two independent replicates) is specified above each
624 graph.
625
626 **Supplementary Figure 6: Two-photon laser ablation efficiently depletes mcMTOCs.**
627 Oocytes expressing AURKA-GFP and eGFP-EB3 were *in vitro* maturated for 6 h (metaphase I,
628 Met I), transferred to CZB medium with MG-132, followed by mcMTOC depletion using two-
629 photon laser ablation. Small square area(s) surrounding mcMTOCs were marked and then
630 exposed to a laser with 927 nm wavelength. Control oocytes were exposed to the same
631 parameters except ablating random areas of the cytoplasm, just adjacent and equal to the same
632 size and number of mcMTOCs. Control and mcMTOC-ablated oocytes were fixed and

633 immunostained using γ-tubulin antibody to label MTOCs. DAPI was used to detect DNA (blue).
634 Arrowheads represent mcMTOCs. Shown are representative Z-projection of confocal images.
635 The scale bar represents 10 μm.
636
637 **Supplementary Movie 1:** Time-lapse confocal microscopy of MTOCs in live oocyte. The
638 full-grown prophase-I oocyte was injected with cRNAs encoding *H2b-mCherry* (red) and *Aurka-*
639 *Gfp* (pseudo grey), followed by *in vitro* maturation. Fluorescence images (Z-projection of 16
640 sections every 3 μm) were captured every 20 min (time, h:min). Same oocyte as shown in Fig.
641 1A (upper panels). The scale bar represents 10 μm.
642
643 **Supplementary Movie 2:** 3D reconstruction of MTOCs from the oocyte in Supplementary
644 Movie 1. Same oocyte as shown in Fig. 1B (lower panels).
645
646 **Supplementary Movie 3:** 3D reconstruction of MTOCs from the oocyte in Supplementary
647 Movie 1 during metaphase I.
648
649 **Supplementary Movie 4:** Time-lapse confocal microscopy of MTOCs in live oocyte. The
650 full-grown prophase-I oocyte was injected with cRNAs encoding *H2b-mCherry* (red) and *Aurka-*
651 *Gfp* (pseudo grey), followed by *in vitro* maturation. Fluorescence images (Z-projection of 16
652 sections every 3 μm) were captured every 15 min (time, h:min). The scale bar represents 20 μm.
653 **Supplementary Movie 5:** Tracking of 3D reconstructed mcMTOCs from the oocyte in
654 Supplementary Movie 4 during nuclear envelope breakdown (NEBD) to early metaphase I (Met
655 I). Same oocyte as shown in Fig. 2A.

Supplementary Movie 6: Tracking of 3D reconstructed mcMTOCs from the oocyte in Supplementary Movie 4 during late metaphase I to telophase I. Same oocyte as shown in Fig. 2C.

Supplementary Movie 7: Time-lapse confocal microscopy of MTOCs in live oocyte. The full-grown prophase-I oocyte was injected with cRNAs encoding *H2b-mCherry* (red) and *Aurka-Gfp* (pseudo grey), followed by *in vitro* maturation. Fluorescence and bright-field images (Z-projection of 16 sections every 3 μm) were captured every 20 min (time, h:min). Same oocyte as shown in Fig. 3C (lower panels). The scale bar represents 10 μm.

Supplementary Movie 8: 3D time-lapse imaging of live oocyte expressing AURKA-GFP (pseudo grey) and eGFP-EB3 (pseudo grey) during mcMTOC ablation. The white squares represent the actual laser beam targets. Same oocyte as shown in Fig. 4B.

Supplementary Movie 9: Tracking the spindle over time in control oocyte (non-mcMTOC-ablated) expressing AURKA-GFP (pseudo grey) and eGFP-EB3 (pseudo grey), while cultured in MG-132-containing medium for 9 h, using 3D time-lapse microscopy. Fluorescence images were captured every 3 min (time, h:min). The scale bar represents 10 μm. Same oocyte as shown in Fig. 4E.

Supplementary Movie 10: Tracking the spindle over time in mcMTOC-laser-ablated oocyte expressing AURKA-GFP (pseudo grey) and eGFP-EB3 (pseudo grey), while cultured in MG-

132-containing medium for 9 h, using 3D time-lapse microscopy. Fluorescence images were captured every 3 min (time, h:min). The scale bar represents 10 μm. Same oocyte as shown in Fig. 4E.

Supplementary Movie 11: Tracking the chromosomes over time in DMSO-treated oocytes during meiosis I. Bright-field images (Z-projection of 16 sections every 3 μm) were captured every 30 min (time, h:min). Prophase -I stage represents 0 h. Same oocyte as shown in Fig. 6A (Control). The scale bar represents 10 μm.

Supplementary Movie 12: Tracking the chromosomes over time in Rapamycin-treated oocytes during meiosis I. Bright-field images (Z-projection of 16 sections every 3 μm) were captured every 30 min (time, h:min). Prophase -I stage represents 0 h. Same oocyte as shown in Fig. 6A (Rapamycin). The scale bar represents 10 μm.

Supplementary Movie 13: Tracking the chromosomes over time in 3-MA-treated oocytes during meiosis I. Bright-field images (Z-projection of 16 sections every 3 μm) were captured every 30 min (time, h:min). Prophase -I stage represents 0 h. Same oocyte as shown in Fig. 6A (3-MA, upper panels). The scale bar represents 10 μm.

Supplementary Movie 14: Tracking the chromosomes over time in 3-MA-treated oocytes during meiosis I (another representative showing defective asymmetrical division). Bright-field images (Z-projection of 16 sections every 3 μm) were captured every 30 min (time, h:min).

701 Prophase -I stage represents 0 h. Same oocyte as shown in Fig. 6A (3-MA, lower panels). The

702 scale bar represents 10 μm.

703

704

705

REFERENCES

1 Von Stetina, J. R. & Orr-Weaver, T. L. Developmental control of oocyte maturation and egg activation in metazoan models. Cold Spring Harb Perspect Biol 3, a005553, doi:10.1101/cshperspect.a005553 (2011).

2 Hashimoto, N. & Kishimoto, T. Regulation of meiotic metaphase by a cytoplasmic maturation-promoting factor during mouse oocyte maturation. Dev Biol 126, 242-252, doi:10.1016/0012-1606(88)90135-2 (1988).

3 Bennabi, I., Terret, M. E. & Verlhac, M. H. Meiotic spindle assembly and chromosome segregation in oocytes. J Cell Biol 215, 611-619, doi:10.1083/jcb.201607062 (2016).

4 Kitajima, T. S., Ohsugi, M. & Ellenberg, J. Complete kinetochore tracking reveals error-prone homologous chromosome biorientation in mammalian oocytes. Cell 146, 568-581, doi:10.1016/j.cell.2011.07.031 (2011).

5 McCarthy, E. K. & Goldstein, B. Asymmetric spindle positioning. Curr Opin Cell Biol 18, 79-85, doi:10.1016/j.ceb.2005.12.006 (2006).

6 Longo, F. J. & Chen, D. Y. Development of cortical polarity in mouse eggs: involvement of the meiotic apparatus. Dev Biol 107, 382-394 (1985).

7 Menezo, Y. J. Paternal and maternal factors in preimplantation embryogenesis: interaction with the biochemical environment. Reprod Biomed Online 12, 616-621, doi:10.1016/s1472-6483(10)61188-1 (2006).

8 Ma, J., Zeng, F., Schultz, R. M. & Tseng, H. Basonuclin: a novel mammalian maternal-effect gene. Development 133, 2053-2062, doi:10.1242/dev.02371 (2006).

9 Schuh, M. & Ellenberg, J. A new model for asymmetric spindle positioning in mouse oocytes. Curr Biol 18, 1986-1992, doi:10.1016/j.cub.2008.11.022 (2008).

10 Azoury, J. et al. Spindle positioning in mouse oocytes relies on a dynamic meshwork of actin filaments. Curr Biol 18, 1514-1519, doi:10.1016/j.cub.2008.08.044 (2008).

11 Li, H., Guo, F., Rubinstein, B. & Li, R. Actin-driven chromosomal motility leads to symmetry breaking in mammalian meiotic oocytes. Nat Cell Biol 10, 1301-1308, doi:10.1038/ncb1788 (2008).

12 McNally, F. J. Mechanisms of spindle positioning. J Cell Biol 200, 131-140, doi:10.1083/jcb.201210007 (2013).

13 Szollosi, D., Calarco, P. & Donahue, R. P. Absence of centrioles in the first and second meiotic spindles of mouse oocytes. J Cell Sci 11, 521-541 (1972).

14 Schuh, M. & Ellenberg, J. Self-organization of MTOCs replaces centrosome function during acentrosomal spindle assembly in live mouse oocytes. Cell 130, 484-498, doi:10.1016/j.cell.2007.06.025 (2007).

15 Xie, B. et al. Poly(ADP-ribose) mediates asymmetric division of mouse oocyte. Cell Res 28, 462-475, doi:10.1038/s41422-018-0009-7 (2018).

16 Schatten, H., Schatten, G., Mazia, D., Balczon, R. & Simerly, C. Behavior of centrosomes during fertilization and cell division in mouse oocytes and in sea urchin eggs. Proc Natl Acad Sci U S A 83, 105-109, doi:10.1073/pnas.83.1.105 (1986).

17 Verlhac, M. H., Lefebvre, C., Guillaud, P., Rassinier, P. & Maro, B. Asymmetric division in mouse oocytes: with or without Mos. Curr Biol 10, 1303-1306 (2000).

18 Clift, D. & Schuh, M. A three-step MTOC fragmentation mechanism facilitates bipolar spindle assembly in mouse oocytes. Nat Commun 6, 7217, doi:10.1038/ncomms8217 (2015).

19 Luksza, M., Queguigner, I., Verlhac, M. H. & Brunet, S. Rebuilding MTOCs upon centriole loss during mouse oogenesis. Dev Biol 382, 48-56, doi:10.1016/j.ydbio.2013.07.029 (2013).
20 Balboula, A. Z. et al. Haspin kinase regulates microtubule-organizing center clustering and stability through Aurora kinase C in mouse oocytes. J Cell Sci 129, 3648-3660, doi:10.1242/jcs.189340 (2016).
21 Breuer, M. et al. HURP permits MTOC sorting for robust meiotic spindle bipolarity, similar to extra centrosome clustering in cancer cells. J Cell Biol 191, 1251-1260, doi:10.1083/jcb.201005065 (2010).
22 Messinger, S. M. & Albertini, D. F. Centrosome and microtubule dynamics during meiotic progression in the mouse oocyte. J Cell Sci 100 (Pt 2), 289-298 (1991).
23 Houliston, E., Pickering, S. J. & Maro, B. Redistribution of microtubules and pericentriolar material during the development of polarity in mouse blastomeres. J Cell Biol 104, 1299-1308, doi:10.1083/jcb.104.5.1299 (1987).
24 Meng, X. Q. et al. Localization of gamma-tubulin in mouse eggs during meiotic maturation, fertilization, and early embryonic development. J Reprod Dev 50, 97-105, doi:10.1262/jrd.50.97 (2004).
25 Maro, B., Houliston, E. & Paintrand, M. Purification of meiotic spindles and cytoplasmic asters from mouse oocytes. Dev Biol 129, 275-282, doi:10.1016/0012-1606(88)90374-0 (1988).
26 Saskova, A. et al. Aurora kinase A controls meiosis I progression in mouse oocytes. Cell Cycle 7, 2368-2376, doi:10.4161/cc.6361 (2008).
27 Solc, P. et al. Aurora kinase A drives MTOC biogenesis but does not trigger resumption of meiosis in mouse oocytes matured in vivo. Biol Reprod 87, 85, doi:10.1095/biolreprod.112.101014 (2012).
28 Bury, L. et al. Plk4 and Aurora A cooperate in the initiation of acentriolar spindle assembly in mammalian oocytes. J Cell Biol 216, 3571-3590, doi:10.1083/jcb.201606077 (2017).
29 Gueth-Hallonet, C. et al. gamma-Tubulin is present in acentriolar MTOCs during early mouse development. J Cell Sci 105 (Pt 1), 157-166 (1993).
30 So, C. et al. A liquid-like spindle domain promotes acentrosomal spindle assembly in mammalian oocytes. Science 364, doi:10.1126/science.aat9557 (2019).
31 Ma, W. & Viveiros, M. M. Depletion of pericentrin in mouse oocytes disrupts microtubule organizing center function and meiotic spindle organization. Mol Reprod Dev 81, 1019-1029, doi:10.1002/mrd.22422 (2014).
32 Mogessie, B. & Schuh, M. Actin protects mammalian eggs against chromosome segregation errors. Science 357, doi:10.1126/science.aal1647 (2017).
33 Brunet, S. & Maro, B. Germinal vesicle position and meiotic maturation in mouse oocyte. Reproduction 133, 1069-1072, doi:10.1530/REP-07-0036 (2007).
34 Almonacid, M. et al. Active diffusion positions the nucleus in mouse oocytes. Nat Cell Biol 17, 470-479, doi:10.1038/ncb3131 (2015).
35 Colin, A. et al. Active diffusion in oocytes nonspecifically centers large objects during prophase I and meiosis I. J Cell Biol 219, doi:10.1083/jcb.201908195 (2020).
36 Almonacid, M. et al. Active Fluctuations of the Nuclear Envelope Shape the Transcriptional Dynamics in Oocytes. Dev Cell 51, 145-157 e110, doi:10.1016/j.devcel.2019.09.010 (2019).

37 Denk, W., Strickler, J. H. & Webb, W. W. Two-photon laser scanning fluorescence microscopy. Science 248, 73-76, doi:10.1126/science.2321027 (1990).

38 Duncan, F. E., Chiang, T., Schultz, R. M. & Lampson, M. A. Evidence that a defective spindle assembly checkpoint is not the primary cause of maternal age-associated aneuploidy in mouse eggs. Biol Reprod 81, 768-776, doi:10.1095/biolreprod.109.077909 (2009).

39 Balboula, A. Z. & Schindler, K. Selective disruption of aurora C kinase reveals distinct functions from aurora B kinase during meiosis in mouse oocytes. PLoS Genet 10, e1004194, doi:10.1371/journal.pgen.1004194 (2014).

40 Watanabe, Y. et al. Autophagy controls centrosome number by degrading Cep63. Nat Commun 7, 13508, doi:10.1038/ncomms13508 (2016).

41 Honda, S. & Shimizu, S. Autophagy controls centrosome number. Oncotarget 8, 14277-14278, doi:10.18632/oncotarget.15362 (2017).

42 George, M. A., Pickering, S. J., Braude, P. R. & Johnson, M. H. The distribution of alpha- and gamma-tubulin in fresh and aged human and mouse oocytes exposed to cryoprotectant. Mol Hum Reprod 2, 445-456, doi:10.1093/molehr/2.6.445 (1996).

43 Roeles, J. & Tsiavaliaris, G. Actin-microtubule interplay coordinates spindle assembly in human oocytes. Nat Commun 10, 4651, doi:10.1038/s41467-019-12674-9 (2019).

44 Schultz, R. M., Montgomery, R. R. & Belanoff, J. R. Regulation of mouse oocyte meiotic maturation: implication of a decrease in oocyte cAMP and protein dephosphorylation in commitment to resume meiosis. Dev Biol 97, 264-273, doi:10.1016/0012-1606(83)90085-4 (1983).

45 Stein, P. & Schindler, K. Mouse oocyte microinjection, maturation and ploidy assessment. J Vis Exp, doi:10.3791/2851 (2011).

46 Tsafriri, A., Chun, S. Y., Zhang, R., Hsueh, A. J. & Conti, M. Oocyte maturation involves compartmentalization and opposing changes of cAMP levels in follicular somatic and germ cells: studies using selective phosphodiesterase inhibitors. Dev Biol 178, 393-402, doi:10.1006/dbio.1996.0226 (1996).

47 Chatot, C. L., Ziomek, C. A., Bavister, B. D., Lewis, J. L. & Torres, I. An improved culture medium supports development of random-bred 1-cell mouse embryos in vitro. J Reprod Fertil 86, 679-688, doi:10.1530/jrf.0.0860679 (1989).

48 Shuda, K., Schindler, K., Ma, J., Schultz, R. M. & Donovan, P. J. Aurora kinase B modulates chromosome alignment in mouse oocytes. Mol Reprod Dev 76, 1094-1105, doi:10.1002/mrd.21075 (2009).

49 Bennabi, I. et al. Artificially decreasing cortical tension generates aneuploidy in mouse oocytes. Nat Commun 11, 1649, doi:10.1038/s41467-020-15470-y (2020).

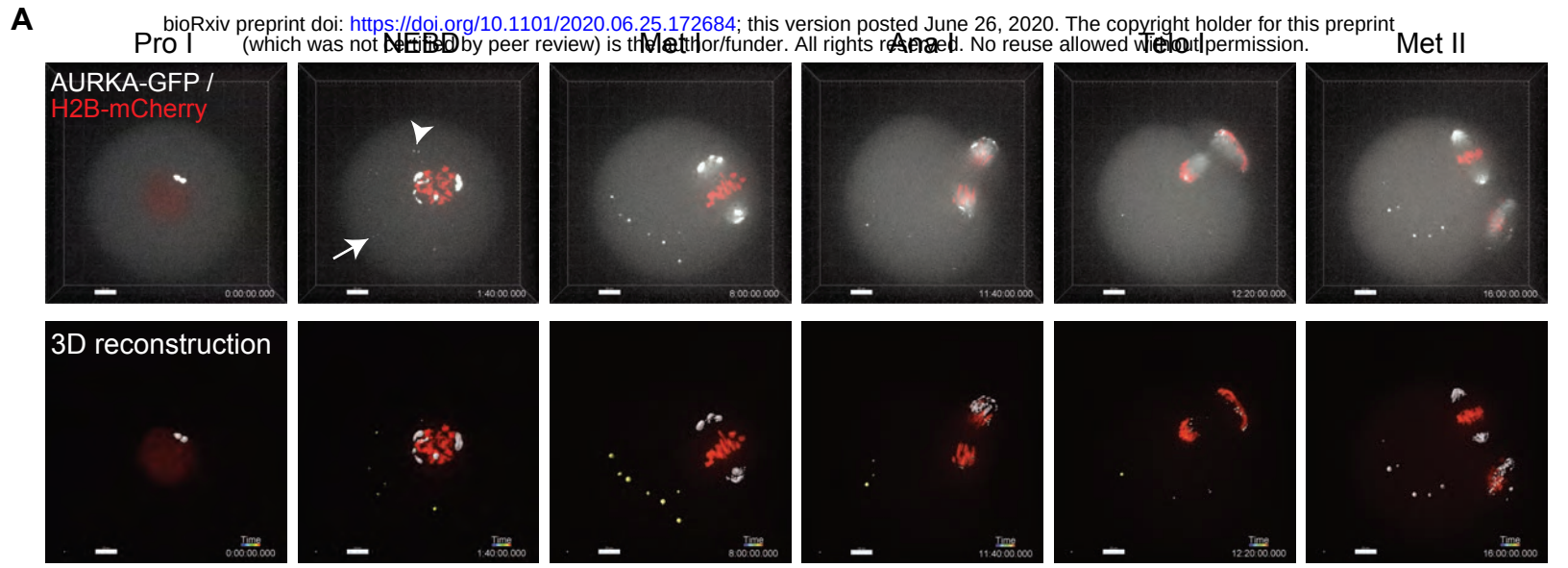

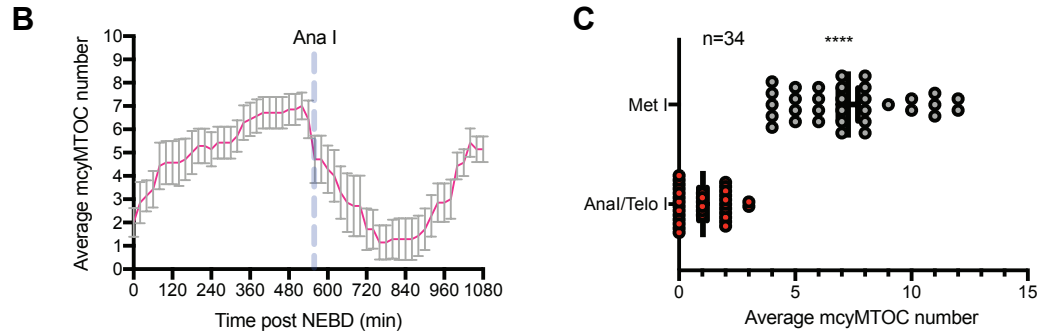

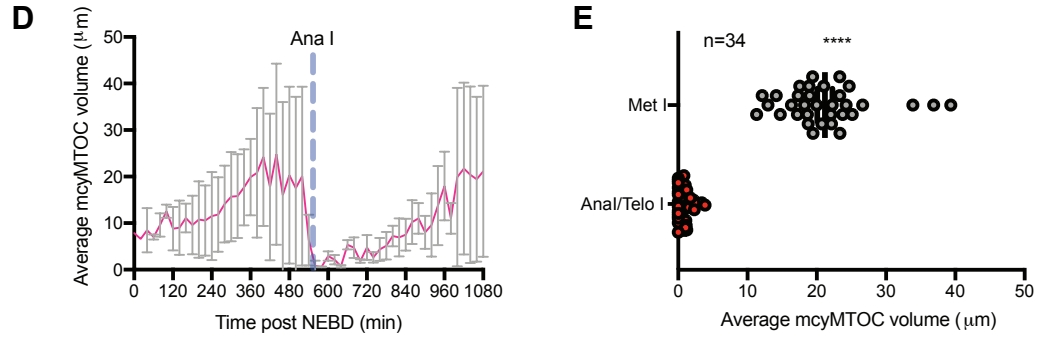

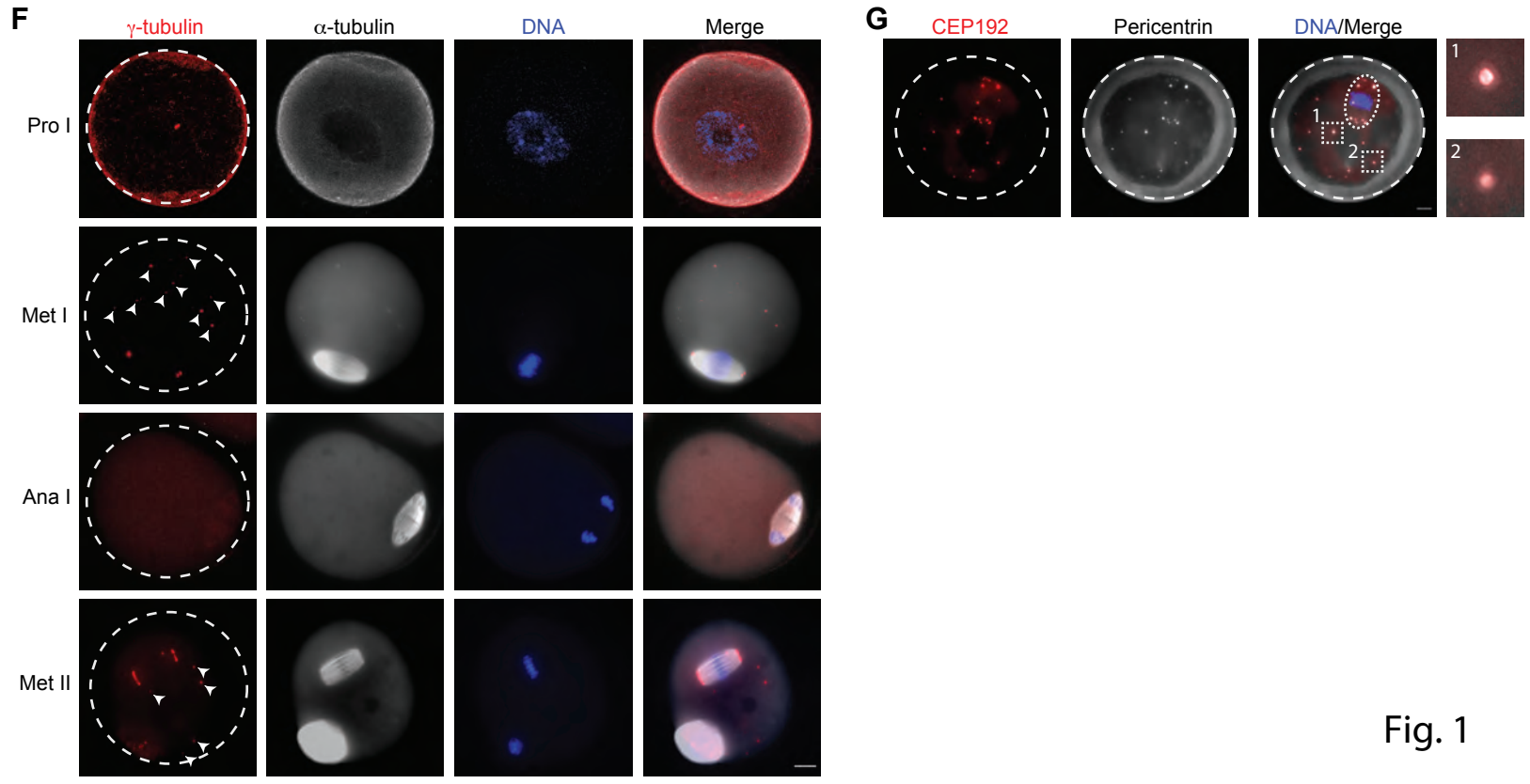

Fig. 1

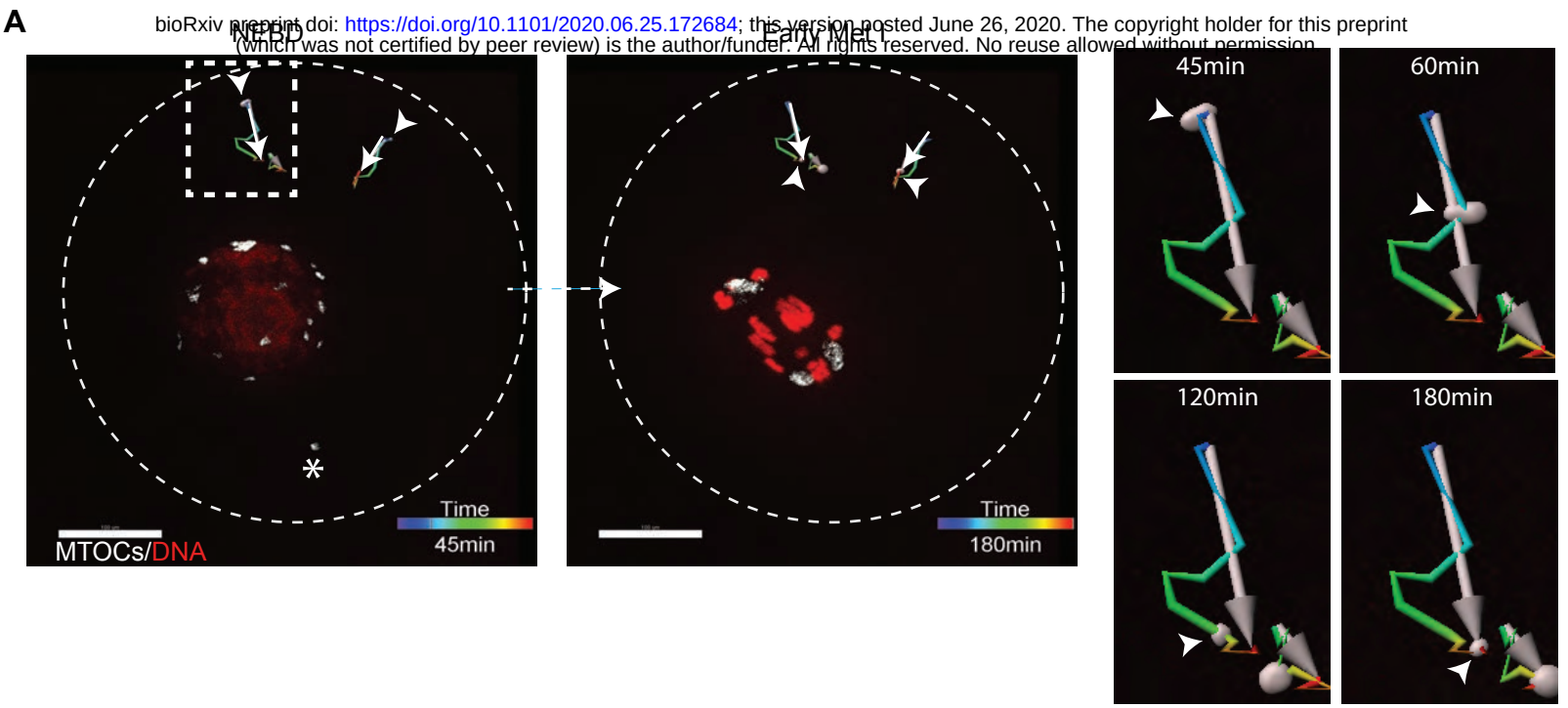

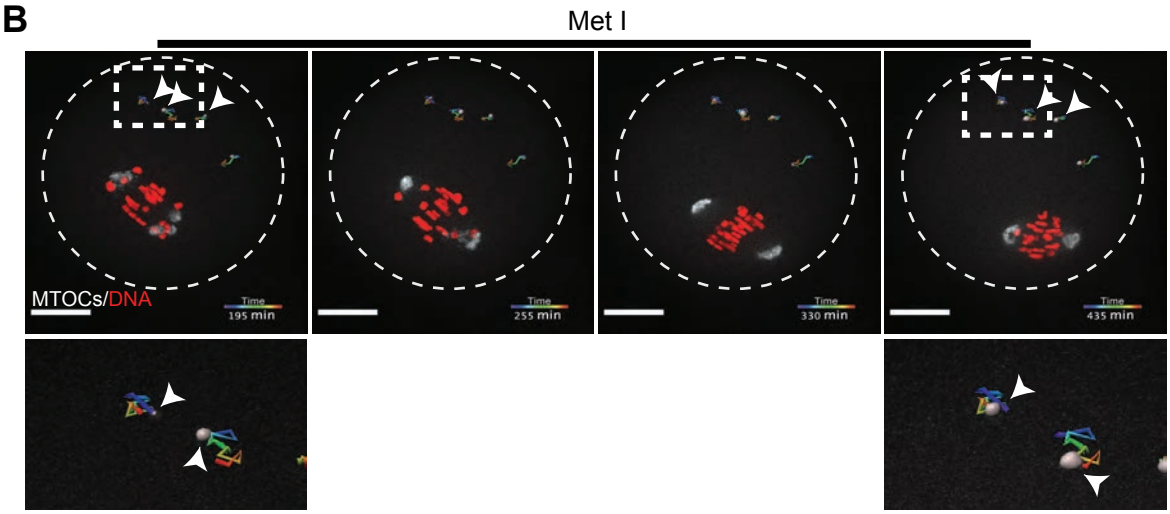

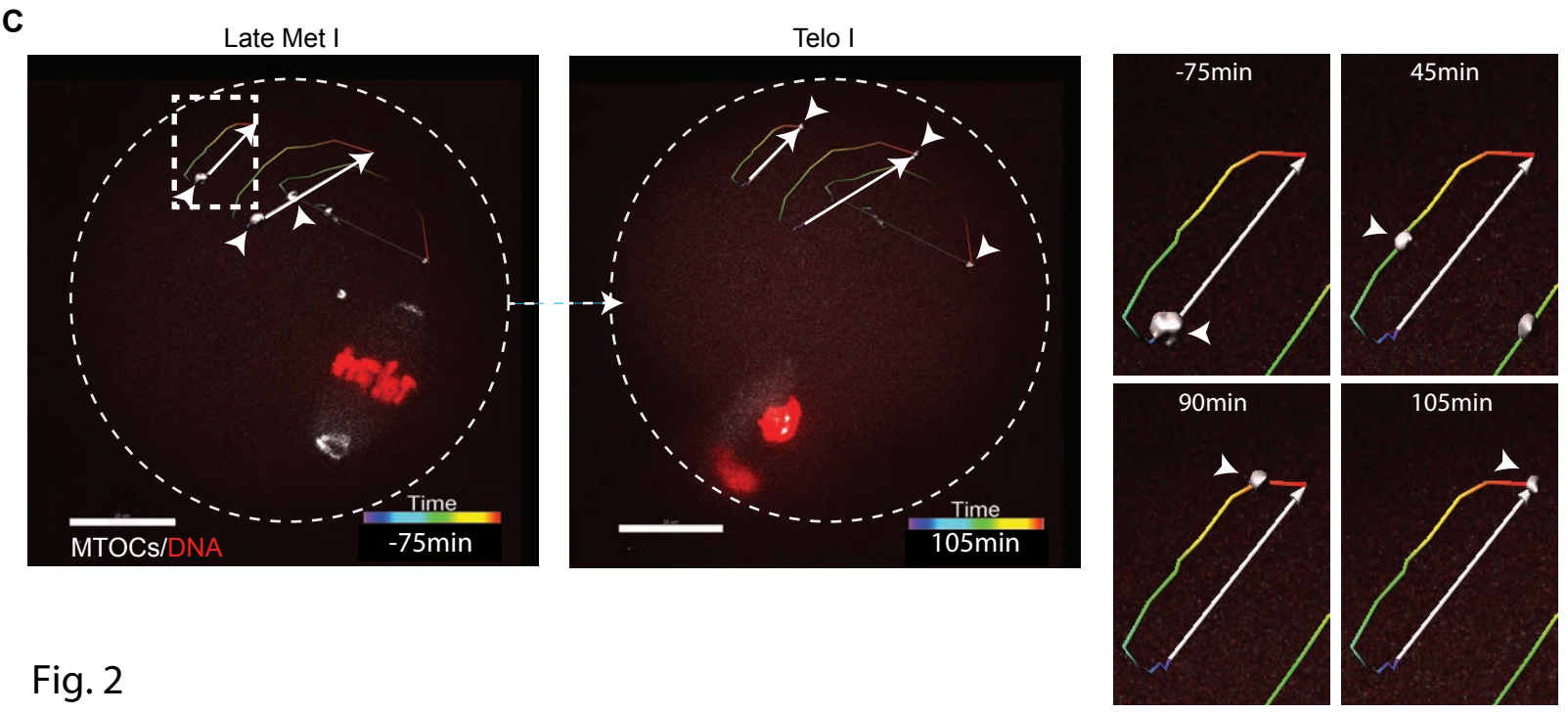

Fig. 2

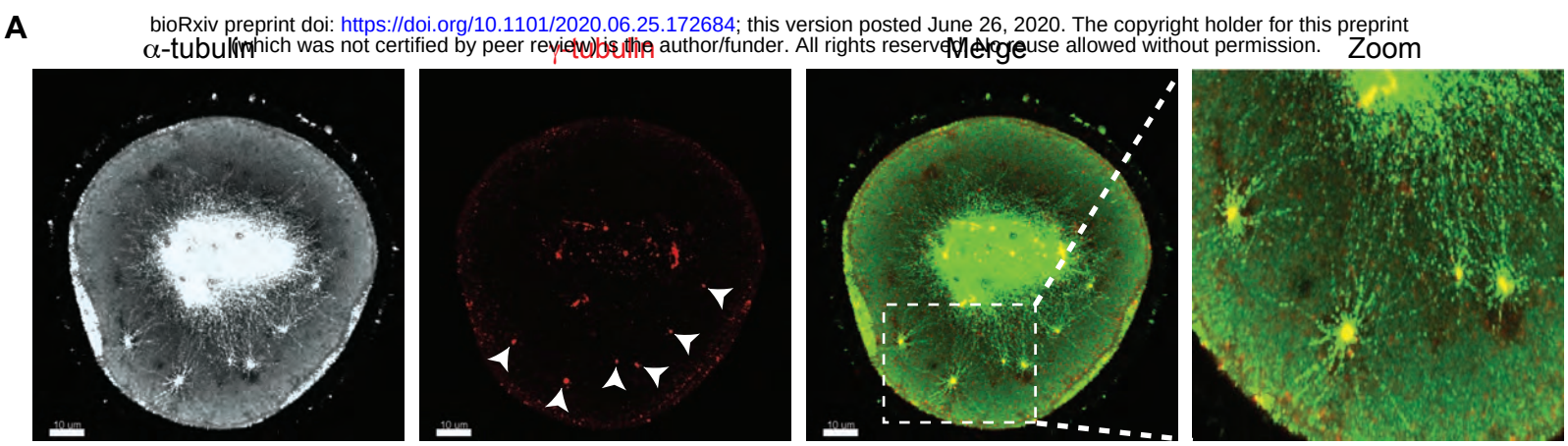

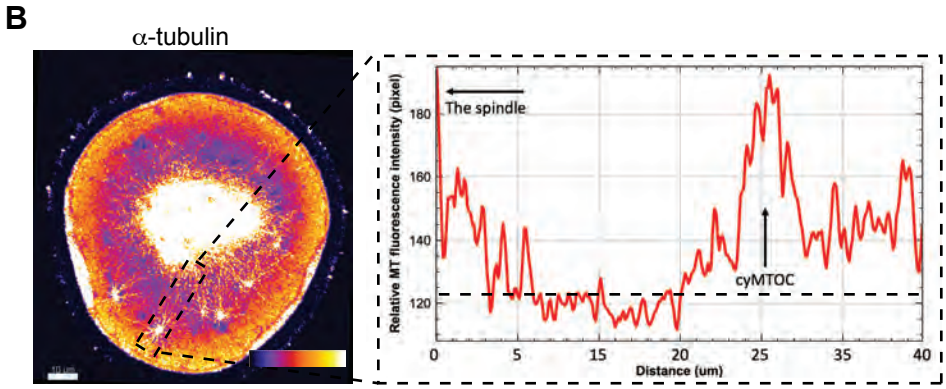

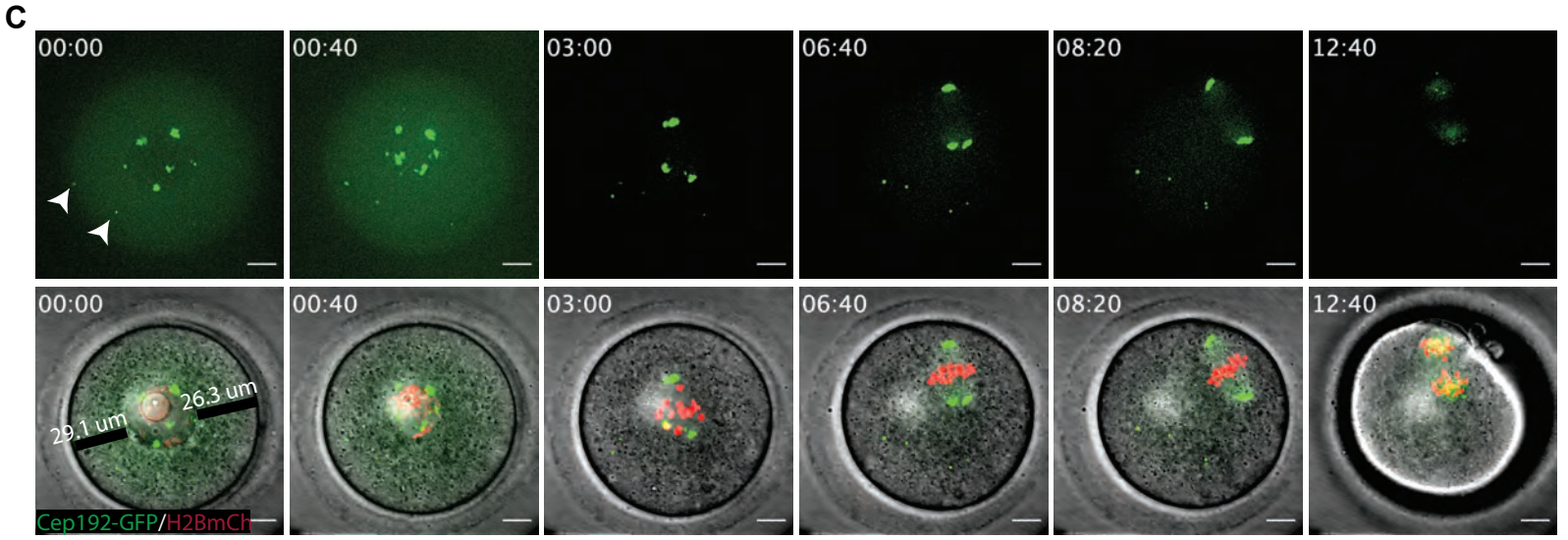

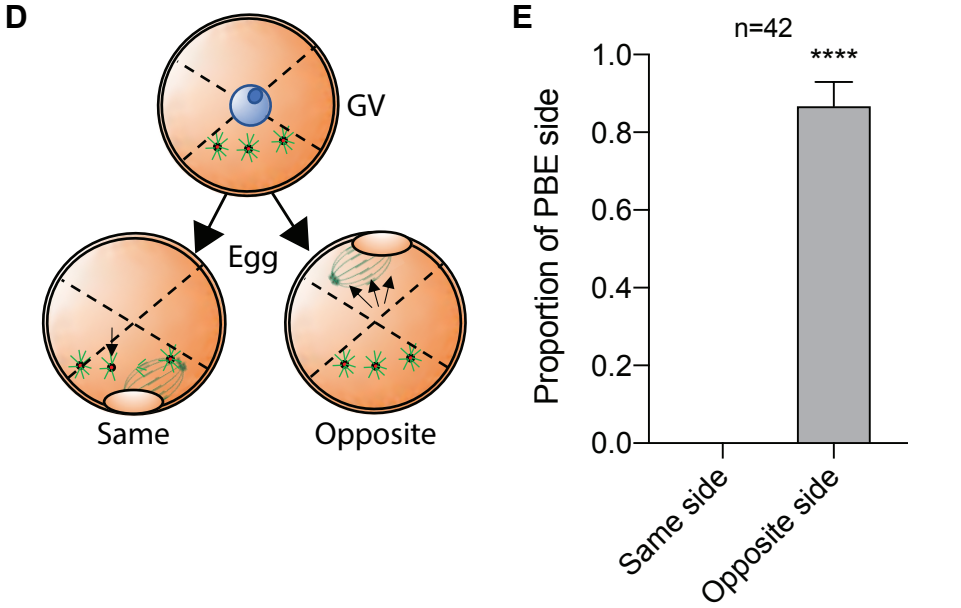

Fig. 3

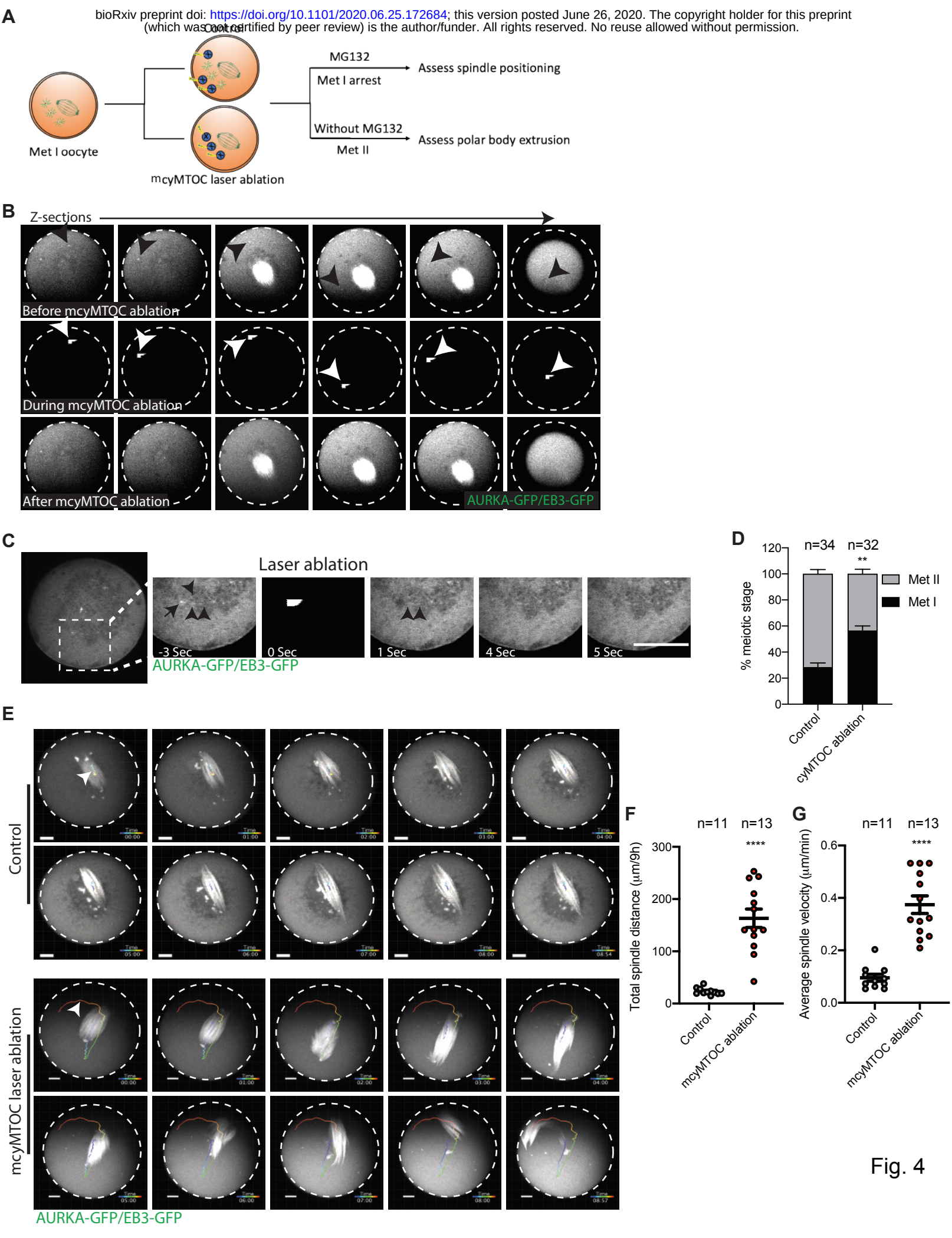

Fig. 4

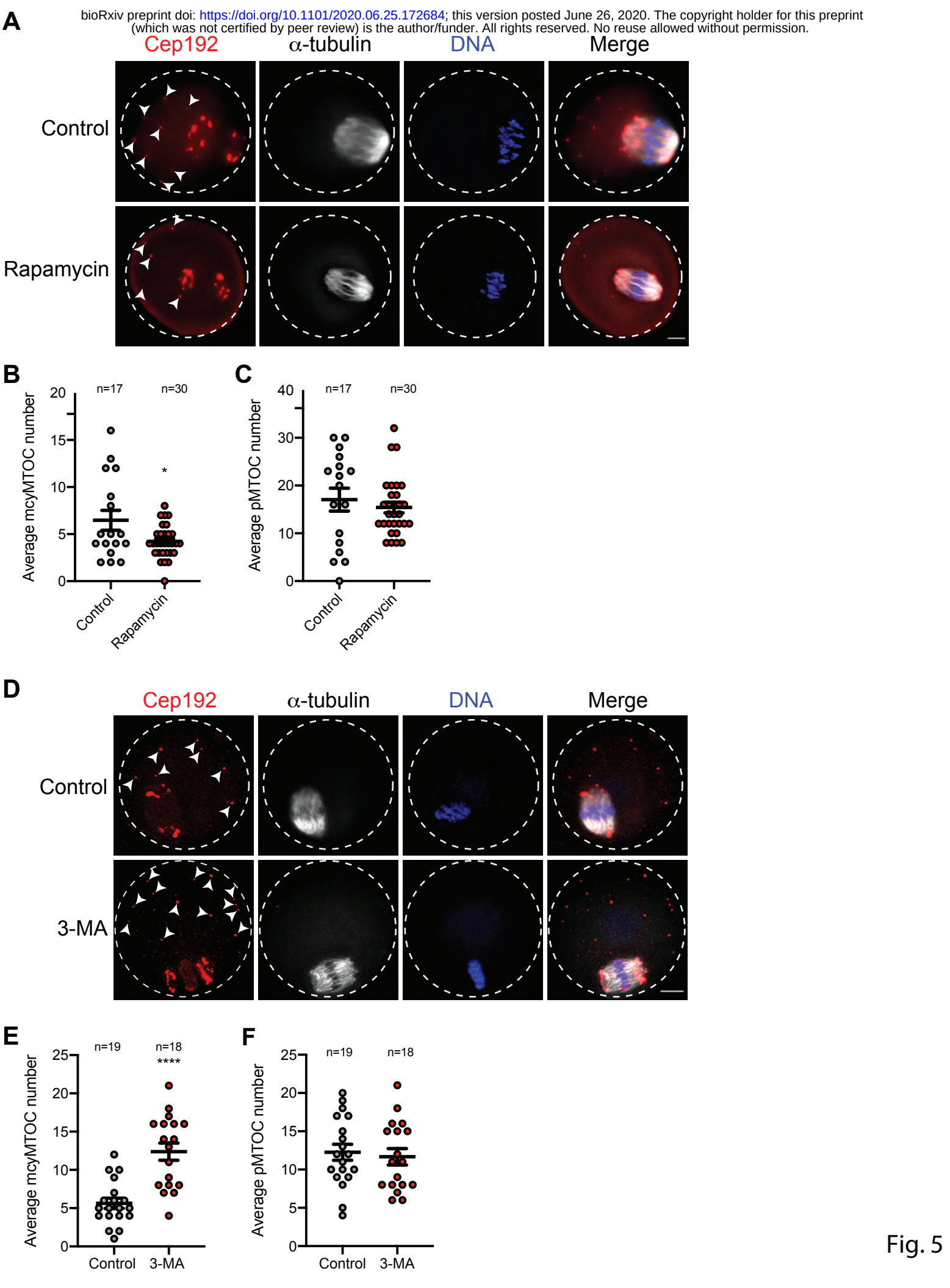

Fig. 5

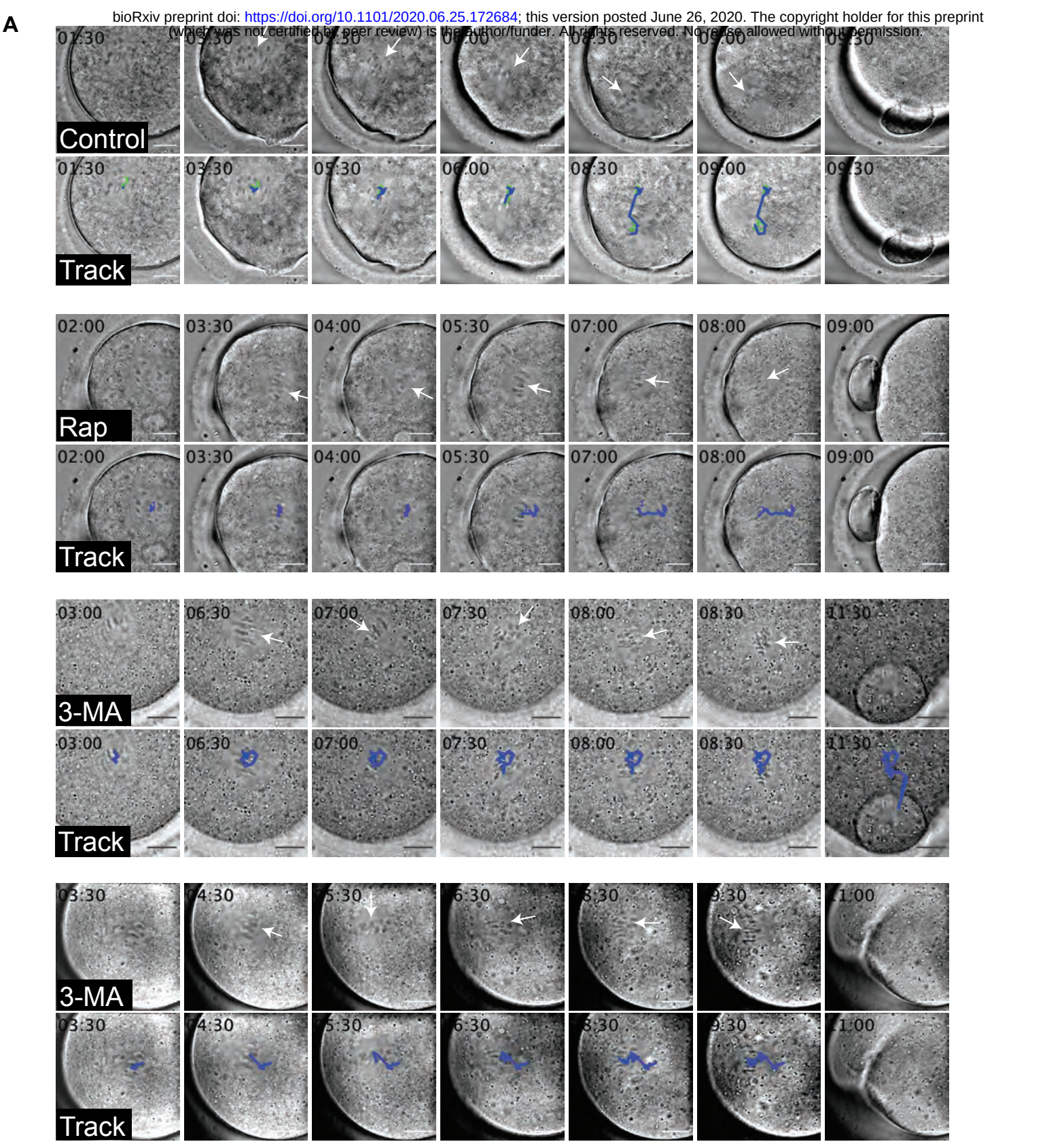

Fig. 6

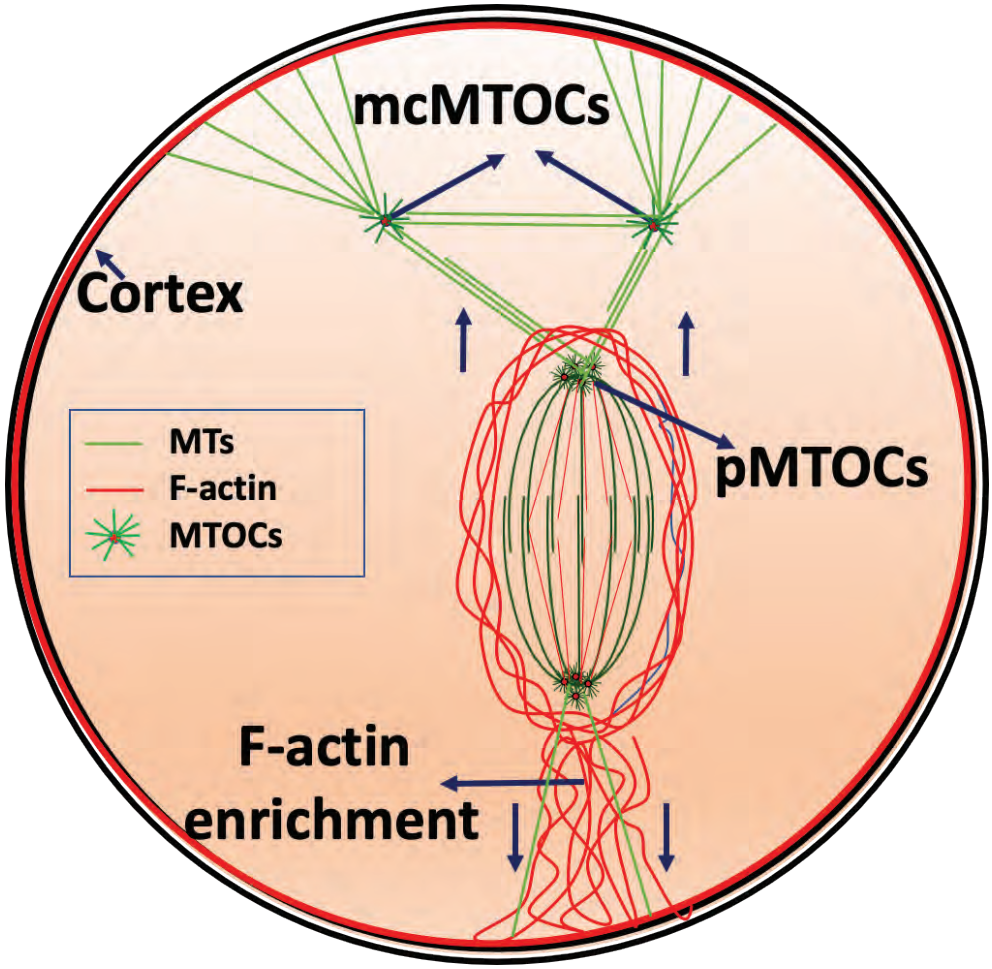

Fig. 7